Research Paper

Effect of Acoustic Enclosure on the Sound Transmission Loss of Multi-Layered Micro-Perforated Plates

Brahim EL KHARRAS* , Mohammed GAROUM , Abdelmajid BYBI

Higher School of Technology in Salé, Material, Energy and Acoustics Team (MEAT)
Mohammed V University in Rabat
Salé, Médina, Morocco

*Corresponding Author e-mail: brahim_elkharras@um5.ac.ma

This study presents an examination of the transmission properties of multilayered partitions made up of multiple micro-perforated plates (MPPs) coupled to acoustic enclosures with general impedance boundaries. Multi-layered MPPs can lower the transmission while minimizing reflection in the source and receiving enclosure. Previous research has mainly focused on the double MPPs or triple MPPs partition itself. However, it is vital to analyze the in-situ sound transmission loss of the multi-layered MPP and their efficiency in a complex vibro-acoustic environment. The case when the multilayered MPPs are coupled to a receiving enclosure or coupled to both a source and receiving enclosure is investigated. The objective is to provide an analytical method to evaluate the transmission properties of multilayered MPPs coupled to acoustic enclosures while being computationally more efficient than the finite element method (FEM). Using the modified Fourier series for the acoustic pressure, a variational form for the acoustic and structure medium yields a completely coupled vibroacoustic system. A comparison between the sound transmission loss of the double MPPs, when mounted on an impedance tube and coupled to acoustics enclosures, shows the modal effect of the enclosures. The effect of enclosure shape, impedance boundary, perforation ratio, air gap thickness on the sound transmission properties of the double MPPs structure is examined for both cases. Finally, in both situations, the performance of triple MPP structure insulation is evaluated.

Keywords: micro-perforated plate (MPP); sound transmission loss; noise insulation; coupled structural-acoustic; surface impedance; modal analysis.

1. Introduction

In recent decades, micro-perforated panels (MPP) have become more popular as a means of noise reduction. In the initial design, the arrangement involved placing perforated panels in front of a solid wall. The purpose was to increase particle velocity through the perforations and dissipate acoustic energy, as documented by MAA (1998). Remarkably, without the need for an additional layer of porous materials, the sub-millimeter-sized holes were capable of providing relatively broad-spectrum absorption. This phenomenon results from the shear forces generated by air vibrations as they pass through these tiny openings. As a result, this design approach facilitates the construction of sound-absorbing walls that are both lightweight and free of fibers, all while maintaining high functionality. MPPs may be utilized as acoustic liners at the intake and exhaust of aircraft nacelles to minimize fan and jet engine noise because of their resistance to degradation and their ability to survive harsh settings where porous materials can degrade. These materials are great for use as outdoor noise barriers, and may even be made out of transparent materials. Therefore, they might be particularly helpful to architects who utilize interior or exterior glass structures (FUCHS, ZHA, 1997), for example, to reduce the long reverberation durations that contribute to poor intelligibility in glass-enclosed spaces. And since environmental considerations are taken into account while creating standards, it is anticipated that in the future, these lightweight, non-polluting, soundproof alterna-

tives, which may be made from recyclable materials, would replace the use of porous barriers.

Micro-perforated panels have also been used in a vast array of other technical applications. Micro-perforated cylinder silencers were the subject of analytical and experimental study by Bravo *et al.* (2016) in the high-sound pressure and low-frequency domains. They examined the nonlinear behavior of a micro-perforated cylinder liner as it dissipated energy and transmitted sound at high pressure. Alisah *et al.* (2021) studied the potential of an expansion chamber coupled micro-perforated cylindrical panel using the boundary element method to enhance the acoustic attenuation for in-duct noise control issues. Yu *et al.* (2015) studied the effectiveness of hybrid silencers made from MPPs and inner partitions, finding that the balance between dissipative and reactive noise attenuation effects could be modified by varying the ideal hole size and perforation ratio, among other aspects. Allam and Åbom (2011) included MPPs in the design of vehicle exhaust mufflers, indicating that mufflers made using MPPs rather than porous materials provide the advantage of a non-fibrous, lighter alternative. Micro-perforated insertion units were developed by Pfretzschner *et al.* (2006) and may be used to protect the acoustic properties of MPPs while reinforcing their fragile thin plates or foils. To increase the frequency range, Liu *et al.* (2017) investigated layered sound absorbers on which a 3D-printed MPP was mounted using a porous sound absorbent material. Yang and Cheng (2016) conducted research on the sound absorption properties of MPPs when supported by either an air volume or a honeycomb structure within small enclosures. Their study revealed that the interaction between the backing cavity and the enclosure had a notable influence on the MPP's ability to absorb sound. Kang and Brocklesby (2005) investigated the viability of utilizing a window arrangement with transparent micro-perforated absorbers and proved that noise could be decreased while enabling much greater airflow compared with traditional window systems. An optimization of the MPP with a multi-depth cavity was carried out by Falsafi and Ohadi (2018) to extend the absorption bandwidth. MPPs have been utilized in honeycomb and corrugated constructions as low-frequency sound-absorbing structures (Meng *et al.*, 2017; 2019; Tang *et al.*, 2017; 2019).

Although sound absorption has been the primary focus of most investigations on MPPs, just a few have studied their sound-isolating properties. Toyoda and Takahashi (2008) examined the acoustic properties of an infinite MPP structure with a back wall. To reduce mid-frequency transmission loss, they performed an analysis of the problem in only two dimensions and proposed an air gap subdivision, namely the use of a structure based on honeycomb. Micro-perforation enhances soundproofing effectiveness at the mass-spring

resonance in the two studies of the soundproofing properties of infinite double and triple windows and panels with micro-perforations (Mu *et al.*, 2011a; 2011b). Sound transmission loss (STL) results of single and double-layered construction with and without micro-perforations were compared by Dupont *et al.* (2003) in their study of lightweight MPP systems. Bravo *et al.* (2012) developed a fully coupled modal approach that predicts the absorption and transmission characteristics of flexible MPP-cavity-plate partitions. The study was expanded (Bravo *et al.*, 2014) and a comparison was conducted between MPP-MPP-plate and MPP-porous-plate partitions. Kim *et al.* (2020a) conducted a comprehensive analysis using the transfer matrix technique to study the impact of micro-perforations on the sound transmission loss (STL) of multi-layered infinite MPPs across the entire frequency spectrum. They employed the concept of equivalent impedance, which combines the impedances associated with both the inertia term and the micro-perforations, as a means to characterize the effects of these perforations. In a related study, Kim *et al.* (2020b) employed the transfer matrix approach while assuming conditions of plane waves in the low-frequency domain. Their investigation centered on analyzing the STL of multi-layered flexible MPPs, which were positioned within a rectangular cross-sectioned impedance tube. Their particular focus was on understanding the behavior of these panels at resonance frequencies.

Analytical and numerical techniques have been utilized to characterize the insulating characteristics of the dividing partition and the parameters that lead to observed differences in the low-frequency range of these qualities to fully explain how finite cavities affect the findings. Kihlman (1967) examined inaccuracies in sound transmission measurement using modal analysis. He noticed that systematic differences may develop in the low-frequency spectrum if the source and receiving rooms have identical dimensions. Other authors (Mulholland, Lyon, 1973; Gagliardini *et al.*, 1991; Kropp *et al.*, 1994; Osipov *et al.*, 1997a; 1997b) have adopted comparable strategies to investigate the impact on the measured low-frequency sound transmission loss such as room size, source location, reverberation duration, interface geometry, or mounting conditions. Bravo and Elliott (2004) introduced a coupled model to investigate systems comprising cavity-panel-cavity and cavity-panel configurations, focusing on the evaluation of low-frequency sound transmission loss. Cheng *et al.* (2005) studied the transmission of energy within double-wall partitions that were mechanically coupled to an acoustic cavity. They specifically examined how the noise insulation characteristics of these structures were affected by factors such as the air gap and mechanical connections, utilizing a fully coupled vibro-acoustic formulation.

We have characterized the double and triple MPPs configurations, as they are of relevance when considering the reduction of the noise transmitted through building walls while providing boundary absorption in the source room and receiving room, lowering their reverberation times and improving the speech intelligibility. In a typical application, multi-layered MPPs might be utilized to reduce transmissions and reflections from both sides compared to the double plate or the plate-cavity-MPP partitions. Multi-layered MPPs behavior must be evaluated in such applications by considering it as a component of the complete system. There are two significant limitations in existing research: (a) the sound transmission of multi-layered MPPs were assessed in simple acoustic environment such as impedance tube or free-field conditions, and (b) the effect of enclosures and boundary conditions on transmission loss the double and triple MPPs structures, when coupled to a receiving enclosure or both the source and receiving enclosure, was not considered. Since these characteristics can greatly alter the transmission properties of multi-layered MPPs, comprehensive knowledge of vibro-acoustic phenomena and their sensitivity to changes in system parameters is of paramount importance. Additionally, the development of a versatile and precise methodology capable of addressing various aspects of systems would greatly benefit both academic researchers and engineers. While numerical approaches such as the finite element method (FEM) are effective for obtaining relevant acoustic data, there is a preference for analytical techniques due to their computational efficiency. Analytical methods are particularly suited for parametric investigations, sensitivity analyses, and optimization. They also serve as reliable benchmarks for the development of acoustic engineering software.

To address the limitations observed in previous models and offer a clearer understanding of the transmission properties of double MPP coupled to acoustic enclosures and their sensitivity to changes in various system parameters, we propose a vibro-acoustic formulation for modeling the behavior of the coupled system. In this proposed approach, we use the modified Fourier series to express the acoustic pressure within the enclosures. Our model assumes a clamped boundary condition, which, while more complex to handle analytically than the simply supported boundary condition, better reflects real-world engineering scenarios in many cases. To obtain solutions for displacement and acoustic pressure, we apply a modified variational principle for the coupled system. Our approach efficiency and accuracy is validated by comparing it with the FEM and impedance tube results. We investigate the impact of key factors on the sound transmission loss of a multi-layered MPP structure when coupled to a receiving acoustic enclosure or both the receiving and source enclosure. These factors include the dimensions of the acoustic enclosure, air gap thickness, acoustic enclosure impedance, plate micro-perforation, and the presence of absorbent materials within the gap. Finally, the case of triple MPPs is also investigated.

2. Theoretical formulations

2.1. Description of the coupled system

Figure 1 illustrates the coupled system under investigation in the present study. This system is a double MPP that is separated by an air gap and coupled to an enclosure cavity. The double MPP structure is composed of two homogeneous and isotropic rectangular micro-perforated plates. The two MPPs are identical. The clamped boundary condition for the MPP is assumed. A uniform, oblique plane sound wave with an incidence elevation angle ϕ and an azimuth angle θ is applied to the top MPP, designated 1, whilst the lower MPP denoted 2, is coupled to a receiving enclosure in the first case. To study the vibro-acoustic behavior of double MPP when coupled to both a source and receiving enclosure, an acoustic point source is placed in a secondary enclosure and coupled to the double MPPs structure in the second case. The air gap and the acoustic enclosures have acoustically rigid walls except for the regions occupied by the two MPPs. Nonetheless, it is worth noting that we can readily introduce an arbitrary impedance surface condition when necessary.
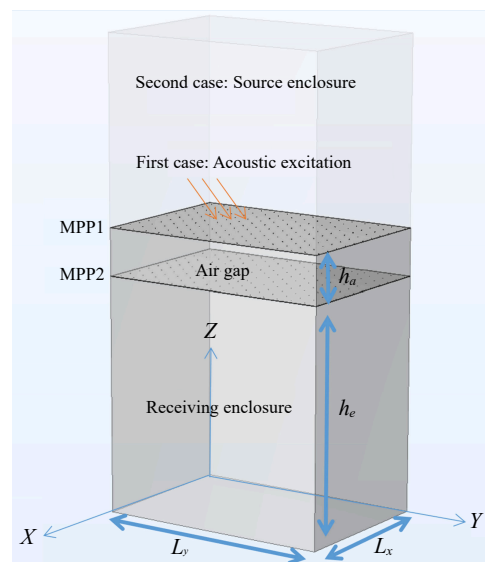
Fig. 1. Schematic of a double micro-perforated plate structure coupled to an enclosure.

The acoustic pressure in the acoustic gap should satisfy both the wave equation and the corresponding boundary conditions.

The wave equation is given as:

$$\nabla^2 p_g + k^2 p_g = 0, \tag{1}$$

where p_g is the acoustic pressure within the acoustic gap, $k = \frac{\omega}{c_0}$ is the wavenumber, and $\nabla^2 = \frac{\partial^2}{\partial x^2} + \frac{\partial^2}{\partial y^2} + \frac{\partial^2}{\partial z^2}$.

The boundary conditions on the air gap boundaries:

$$\frac{\partial p_g}{\partial z} = j\omega\rho_0\overline{v}_1, \qquad \text{on MPP1}, \qquad (1)_1$$

$$\frac{\partial p_g}{\partial z} = -j\omega\rho_0\overline{v}_2, \qquad \text{on MPP2}, \qquad (1)_2$$

$$\frac{\partial p_g}{\partial n} = 0, \qquad Z(\omega) = \infty, \qquad \text{on the rigid wall}, \quad (1)_3$$

where ρ_0 and c_0 are the density of air and the speed of sound, respectively, and $\overline{v}_j$ is the average velocity of the j-th MPP.

Similarly, the acoustic pressure within the enclosure satisfies the wave equation including the continuity conditions on the boundaries:

$$\nabla^2 p_e + k^2 p_e = 0,$$

$$\frac{\partial p_e}{\partial z} = j\omega\rho_0\overline{v}_2, \qquad \text{on MPP2}, \qquad (2)$$

$$\frac{\partial p_e}{\partial z} = -j\omega\rho_0\frac{p_e}{Z}, \qquad \text{on the walls},$$

where p_e is the acoustic pressure inside the enclosure.

As can be seen in Fig. 2, the average velocity $\overline{v}$ of the MPP is related directly to the velocity of the plate v_p as well as the velocity of the fluid v_f as it passes through the hole:

$$\overline{v} = v_p(1-\sigma) + v_f\sigma, \qquad (3)$$

where σ denotes the perforation ratio, and it is defined as $\sigma = \pi d^2/4U^2$, where d denotes the hole's diameter and U represents the distance between the holes of the MPP.
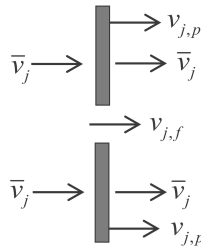
Fig. 2. Average velocity on the surface of the j-th MPP.

As was shown in prior research (TAKAHASHI, TANAKA, 2002), the impedance of the MPP is related to the pressure difference:

$$Z_{\text{resist}}(v_f - v_p) + Z_{\text{react}}v_f = \Delta p. \qquad (4)$$

According to MAA (1998), the impedance of the hole, $Z = Z_{\text{resist}} + Z_{\text{react}}$, which consist of a resistive part and an imaginary part. The former corresponds to the resistive force between the fluid and the inner surface of the hole and the latter deals with the inertia force (motion) of the fluid in the hole. They are given as:

$$Z_{\text{resist}} = \frac{8\eta_0 h}{(d/2)^2}\left(\sqrt{1 + \frac{X^2}{32}} + \frac{\sqrt{2}\,dX}{32h}\right), \qquad (5)$$

$$Z_{\text{react}} = j\rho\omega h\left(1 + \frac{1}{\sqrt{9 + \frac{X^2}{2}}} + \frac{8d}{3\pi h}\right), \qquad (6)$$

where η_0 represents the air's viscosity coefficient, h denotes the thickness of the MPP, and $X = \left(\frac{d}{2}\right)\sqrt{\frac{\rho\omega}{\eta}}$.

When we eliminate $v_{j,f}$ from Eqs. (3) and (4), we get the relation:

$$\overline{v} = \gamma v_p + \frac{\sigma\Delta p}{Z}, \qquad (7)$$

in which

$$\gamma = 1 - \sigma\left(\frac{Z_{\text{react}}}{Z}\right). \qquad (8)$$

For the first MPP, $\Delta p_1 = p_0 - p_g$.

The governing equation of the first MPP is given as a function of MPP displacement w_1 (and $v_{1,p} = j\omega w_1$):

$$D_1\nabla^4 w_1 - M_1\omega^2 w_1 = p_0 - p_g, \qquad (9)$$

where M_1 is the mass per unit area and D_1 is the flexural rigidity of the first MPP, it can be written as:

$$D_1 = E_1 h_1^3/12(1 - v_1^2), \qquad (10)$$

where E_1 represent Young's modulus, v_1 is Poisson's ratio, and h_1 is the thickness.

In Eq. (10), damping of the structure is taken into consideration by inserting complex Young's modulus $E(1 + j\eta)$, where η is the loss factor.

The sound pressure acting on the incident panel consists of three distinct pressures: the incident pressure, the reflected pressure, and the radiated pressure. Among these three components, the radiated pressure is notably negligible. This is primarily due to the incident plate's impedance is comparable to that of a rigid boundary when subjected to air loading. Consequently, it is reasonable to assume that the magnitudes of the incident and reflected pressure waves are equal (CARNEAL, FULLER, 2004; CHAZOT, GUYADER, 2007).

Hence, in cases involving light fluid-loading and sub-millimetric holes with substantial resistive effects, neglecting the radiated pressure directed outward and assuming equivalence in magnitude between the incident and reflected pressures, we can conclude that the blocked pressure, often referred to as the excitation pressure, is twice the magnitude of the incident wave:

$$p_0(x,y,t) = 2p_{\text{inc}}\exp\left(j\omega t - jkz\cos(\phi)\right.$$

$$\left. - jky\sin(\phi)\sin(\theta) - jkx\sin(\phi)\cos(\theta)\right). \quad (11)$$

In the same manner, the governing equation of the second MPP is given as a function of the MPP displacement w_2 (and $v_{2,p} = j\omega w_2$):

$$D_2 \nabla^4 w_2 - M_2 \omega^2 w_2 = p_g - p_e, \tag{12}$$

where M_2 is the mass per unit area and D_2 is the flexural rigidity of the second MPP.

2.2. Solution procedure of the coupled system

Under the assumption that the double MPP are fully clamped, the transverse deflection and moment rotation of each panel are constrained to remain zero along their edges. Consequently, their transverse displacements can be expressed as:

$$w_{j,p}(x,y) = \sum_{m,n} q_{j,mn} \varphi_{mn}(x,y), \tag{13}$$

where the modal functions φ_{mn} or, more strictly speaking, the basic functions take the following forms (XIN et al., 2008):

$$\varphi_{mn}(x,y) = \left(1 - \cos\left(\frac{2m\pi x}{L_x}\right)\right)\left(1 - \cos\left(\frac{2n\pi y}{L_y}\right)\right). \tag{14}$$

Note that the clamped modal function of Eq. (13) is different from the simply supported modal function $\varphi_{mn}(x,y) = \sin\left(\frac{2m\pi x}{L_x}\right)\sin\left(\frac{2n\pi y}{L_y}\right)$.

To ensure differential continuity at the structural-acoustic coupling interface, the sound field inside the enclosure and the air gap may be represented (DU et al., 2011):

$$p_g(x,y,z) = \sum_{m_x=0}^{M_x} \sum_{m_y=0}^{M_y} \sum_{m_z=0}^{M_z} A^g_{m_x m_y m_z}$$
$$\cdot \cos(\lambda_{m_x} x) \cos(\lambda_{m_y} y) \cos(\lambda_{m_z} z)$$
$$+ \sum_{m_x=0}^{M_x} \sum_{m_y=0}^{M_y} (\xi_{1L_z}(z) a^g_{m_x m_y} + \xi_{2L_z}(z) b^g_{m_x m_y})$$
$$\cdot \cos(\lambda_{m_x} x) \cos(\lambda_{m_y} y), \tag{15}$$

$$p_e(x,y,z) = \sum_{m_x=0}^{M_x} \sum_{m_y=0}^{M_y} \sum_{m_z=0}^{M_z} A^e_{m_x m_y m_z}$$
$$\cdot \cos(\lambda_{m_x} x) \cos(\lambda_{m_y} y) \cos(\lambda_{m_z} z)$$
$$+ \sum_{m_x=0}^{M_x} \sum_{m_y=0}^{M_y} \xi_{2L_z}(z) b^e_{m_x m_y}$$
$$\cdot \cos(\lambda_{m_x} x) \cos(\lambda_{m_y} y), \tag{16}$$

where $\lambda_{m_s} = \frac{m_s \pi}{L_s}$, $(s = x, y, z)$. The supplemental functions $\xi_{1L_s}(s)$ and $\xi_{2L_s}(s)$ can be found in (DU et al., 2011).

Theoretically, an acoustic analysis of a cavity can be formulated using a variational approach. This approach can yield a solution that is more advantageous compared to simply solving the Helmholtz equation. To achieve this objective, a modified variational approach (CHIEN, 1983; QU et al., 2013a; 2013b) is employed to define the distribution of sound pressure. This technique involves seeking the minimum value of the corresponding modified variational function:

$$\iiint_{V_g} \frac{1}{2} \left[p_g \frac{jk}{\rho_0 c_0} p_g - (\nabla p_g)^{\mathrm{T}} \frac{j}{\rho_0 \omega} (\nabla p_g) \right] \mathrm{d}V$$
$$+ \iint_{S_{\mathrm{MPP1}}} p_g \overline{v}_1 \, \mathrm{d}S - \iint_{S_{\mathrm{MPP2}}} p_g \overline{v}_2 \, \mathrm{d}S = 0. \tag{17}$$

Using Eq. (17) we get:

$$\iiint_{V_g} \frac{1}{2} \left[p_g \frac{jk}{\rho_0 c_0} p_g - (\nabla p_g)^{\mathrm{T}} \frac{j}{\rho_0 \omega} (\nabla p_g) \right] \mathrm{d}V$$
$$+ \iint_{S_{\mathrm{MPP1}}} p_g \left(\gamma_1 v_{1,p} + \frac{\sigma_1 \Delta p_1}{Z_1} \right) \mathrm{d}S$$
$$- \iint_{S_{\mathrm{MPP2}}} p_g \left(\gamma_2 v_{2,p} + \frac{\sigma_2 \Delta p_2}{Z_2} \right) \mathrm{d}S = 0, \tag{18}$$

where $\Delta p_1 = p_0 - p_g$ and $\Delta p_2 = p_g - p_e$.

The characteristic equation may be found by inserting the admissible function specified in Eqs. (13), (15), and (16) into Eq. (18), and then carrying out the variational operation in terms of the generalized coordinate vector.

The resultant equation for the air gap is as:

$$[K_g + j\omega Z_g + \omega^2 M_g] P_g + \omega^2 C_{p_g,w_1} W_{\mathrm{MPP1}}$$
$$- \omega^2 C_{p_g,w_2} W_{\mathrm{MPP2}} + j\omega C_{p_g,p_e} P_g = j\omega \{P_{0,w_1}\}. \tag{19}$$

In the same manner, for the acoustic enclosure, we get:

$$\left[K_e + j\omega Z_e + \omega^2 M_e \right] P_e + \omega^2 C_{p_e,w_2} W_{\mathrm{MPP2}}$$
$$+ j\omega C_{p_e,p_g} P_g = \{0_e\}. \tag{20}$$

By setting the integral of a weighted residual of the modal function to zero, an arbitrarily accurate double series solution can be obtained. For the current double MPPs partition system, the integral equations are:

$$\iint_{S_{\mathrm{MPP_1}}} (D_1 \nabla^4 w_1 - M_1 \omega^2 w_1) \varphi_{mn}(x,y) \, \mathrm{d}x \, \mathrm{d}y$$
$$= \iint_{S_{\mathrm{MPP_1}}} p_0 \varphi_{mn}(x,y) \, \mathrm{d}x \, \mathrm{d}y$$
$$- \iint_{S_{\mathrm{MPP_1}}} p_g \varphi_{mn}(x,y) \, \mathrm{d}x \, \mathrm{d}y, \tag{21}$$

$$\iint\limits_{S_{\mathrm{MPP}_2}} (D_2 \nabla^4 w_2 - M_2 \omega^2 w_2)\varphi_{mn}(x,y)\,\mathrm{d}x\,\mathrm{d}y$$

$$= \iint\limits_{S_{\mathrm{MPP}_2}} p_g \varphi_{mn}(x,y)\,\mathrm{d}x\,\mathrm{d}y$$

$$- \iint\limits_{S_{\mathrm{MPP}_2}} p_e \varphi_{mn}(x,y)\,\mathrm{d}x\,\mathrm{d}y. \qquad (22)$$

By substituting Eqs. (13), (15), and (16) into Eqs. (21) and (22) and subsequently engaging in meticulous yet straightforward algebraic manipulations, the matrix equations for the MPPs are derived:

$$[K_{p_1} + \omega^2 M_{p1}]W_{\mathrm{MPP1}}$$
$$+ C_{p_g, w_1}^{\mathrm{T}} P_g = \{P'_{0, w_1}\}, \quad (23)$$

$$[K_{p_2} + \omega^2 M_{p_2}]W_{\mathrm{MPP2}} - C_{p_g, w_2}^{\mathrm{T}} P_g$$
$$+ C_{p_e, w_2}^{\mathrm{T}} P_e = \{0\}. \qquad (24)$$

The enclosure and the air gap Eqs. (19) and (20) and the MPPs Eqs. (23) and (24) form a set $(N_e + N_g + M_{\mathrm{MPP1}} + M_{\mathrm{MPP2}})$ of coupled equations that may be put in matrix form as:

$$[\mathbf{K} + j\omega C + \omega^2 \mathbf{M}]\mathbf{X} = \mathbf{Q}, \qquad (25)$$

where $\mathbf{M}$ and $\mathbf{K}$ are diagonal matrices representing the mass and stiffness of the whole system, respectively, and $\mathbf{X}$ is the vector of the unknown complex modal amplitudes. The MPP and cavity modal components that couple with the external pressure are correspondingly represented by the generalized excitation vector $\mathbf{Q}$.

To study the effect of a source room on the transmission properties of multi-layered MPPs. The previous theoretical formulations could also be extended to include a secondary acoustic enclosure as a source room.

The acoustic pressure in the emitting enclosure satisfies the wave equation including the continuity conditions on the boundaries:

$$\nabla^2 p_s + k^2 p_s = j\omega\rho_0 Q\delta(x-x_0)(y-y_0)(z-z_0),$$
$$\frac{\partial p_s}{\partial z} = j\omega\rho_0 \overline{v}_1, \qquad (26)$$

where p_s is the acoustic pressure inside the enclosure, Q is the source strength, and (x_0, y_0, z_0) is the position of the acoustic source.

Similarly making use of the modified Fourier series for the acoustic pressure and then carrying out the variational operation in terms of the generalized coordinate vector. A new set $(N_s + N_e + N_g + M_{\mathrm{MPP1}} + M_{\mathrm{MPP2}})$ of coupled equations can be obtained.

2.3. Sound transmission loss

The transmission loss or sound reduction index of a double MPP connected to a receiving enclosure is defined by:

$$\mathrm{TL} = 10\log_{10}\left(\frac{\Pi_{\mathrm{inc}}}{\Pi_{\mathrm{rad}}}\right) \text{ [dB]}, \qquad (27)$$

where Π_{inc} and Π_{rad} are the sound power incident and radiated by the double MPP structure, respectively, at a given frequency.

The incident acoustic power can be defined as:

$$\Pi_{\mathrm{inc}} = \frac{1}{2}\mathrm{Re}\iint\limits_{A} p_i . v_i^* \,\mathrm{d}A. \qquad (28)$$

The conjugate of a complex variable is denoted by $*$, v_i is the acoustic velocity, and p_i the incident sound pressure. When the incident wave is plane and the acoustic medium is air, the incident power is (Chazot, Guyader, 2007; Xin *et al.*, 2008):

$$\Pi_{\mathrm{inc}} = \frac{p_i^2 \cos(\varphi).S}{2\rho_0 c_0}. \qquad (29)$$

The potential energy in the receiving enclosure is used to compute the partition's radiated power.

In the second case where the multilayered MPPs are connected to both a receiving and the source room, we define the sound transmission loss as (Løvholt *et al.*, 2017):

$$\mathrm{STL} = 20\log_{10}\left(\frac{|p_{\mathrm{re}}|}{|p_{\mathrm{so}}|}\right), \qquad (30)$$

where $|p_{\mathrm{re}}|$ and $|p_{\mathrm{so}}|$ are the absolute values of the pressure averaged over the receiving room and the source room, respectively.

3. Numerical model

The numerical model is constructed using COMSOL Multiphysics. In this model, a plane wave is applied to the incident section. The air in the incident field, receiving enclosure, and air gap is considered to be compressible, with no consideration for thermal conductivity or viscosity. Therefore, the pressure acoustics module within COMSOL, which is suitable for all frequency-domain simulations, is employed.

During the simulation, the MPP are represented as isotropic linear elastic materials using COMSOL's Solid Mechanics module. It is important to note that the simulation accounts for the thermal conduction and viscosity of the air within the small pores. To handle this, the thermal-acoustics module is utilized.

In the case where a source enclosure is coupled to the multilayered MPPs, the incident field is replaced by an enclosure and the pressure acoustics module is employed.

3.1. Boundary conditions

In the finite element (FE) model, it is assumed that at the interface between the pressure acoustic

field and the solid panel, the normal accelerations of the air and the panel are equal. Furthermore, the FE model enforces continuous normal stress, acceleration, and adiabatic conditions at the interface between the thermal acoustic field and the pressure acoustic field. Additionally, the air velocity at the interface between the thermal acoustic field and the solid panel coupling boundary is set to be equal to the velocity of the panel, and temperature variation is treated as isothermal.

The FE model also takes into account the boundary conditions of the MPP, the acoustic enclosure, and the air gap. Tetrahedral elements are used to mesh the FE model, as depicted in Fig. 3. It is important to note that the dimensions of each part have an impact on the size of the elements used in the model.
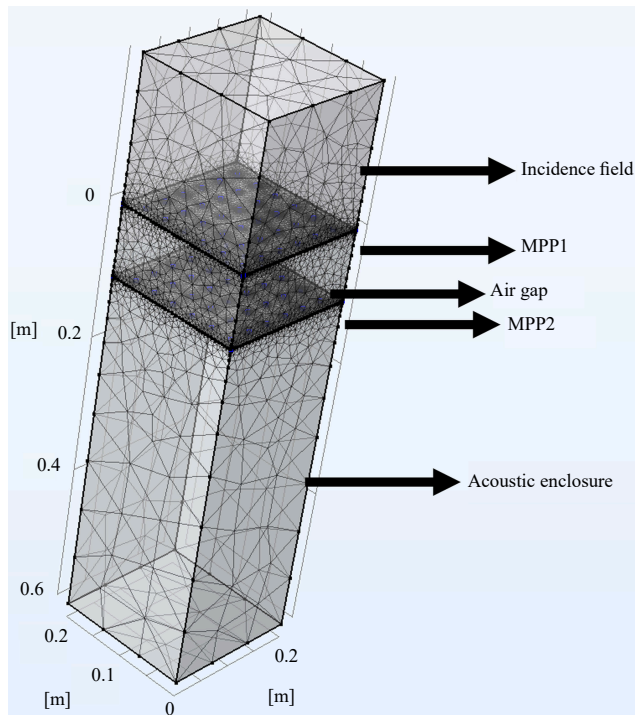
Fig. 3. FE model of a double MPP coupled to an acoustic enclosure.

4. Numerical results and discussions

In this section, the model is validated and a parametric study is conducted by the theoretical modeling and solution approach outlined in the preceding sections of the paper. Comparison between the STL of the double MPP structure, in both cases, obtained using the current approach and FEM is carried out first to assess the limit of applicability and verify its reliability and accuracy. Then, parametric research on the effect of the coupled system parameters on the sound transmission loss is also carried out, including acoustic enclosure dimension and impedance, micro-perforation of the MPPs, air gap thickness, and the influence of the absorbent material introduced in the gap.

4.1. Validation of the analytical formulation

The numerical precision and accuracy of the analytical formulation are assessed on a double MPP connected to a receiving enclosure and both a source and receiving enclosure.

In this study, we consider MPPs made of aluminum plates with the following material properties: Young's modulus $E = 7.2 \times 10^{10}$ Pa, Poisson's ratio $v = 0.34$, density $\rho_p = 2700$ kg/m^3, and the loss factor is assumed to be $\eta = 0.01$. The sidewalls around the air gap cavity and the enclosure are perfectly rigid. The properties of air are $\rho_0 = 1.2$ kg/m^3 and $c_0 = 343$ m/s, and the viscosity is $\eta_0 = 17.9 \times 10^{-6}$ kg/m·s. The flexible MPPs have a dimension of 0.2 m $\times 0.2$ m, and 1 mm thick. The depth of the air gap (h_a) and the receiving enclosure (h_e) considered are 0.1 and 0.5 m, respectively. In the case when the double MPPs structure is connected to both a receiving and source enclosure, a point source of strength $Q_0 = 10^{-4}$ m^3/s placed at $(0.15, 0.12, 0.4)$ in the source enclosure. The dimensions of the source enclosure are: $L_x \times L_y \times h_{e2} = 0.2$ m $\times 0.2$ m $\times 0.6$ m.

The clamped boundary conditions for both the flexible MPPs are considered in the present solution technique. The MPP parameters are $\sigma_1 = \sigma_2 = 0.1\%$ and $d_1 = d_2 = 0.8$ mm.

The primary factor influencing the accuracy of the solution is the number of modes employed for decomposing both displacement and acoustic pressure. To ensure the calculation accuracy, the number of modal truncations (N) and (M) is checked for both the structural and acoustic domains based on the FE calculation results. Typically, precision can be enhanced by increasing the number of modes until convergence is obtained within the desired frequency range. For the dimensions of the coupled system, when $N_1 = N_2 = 7$ and $M_x = M_y = M_z = 4$, a satisfactory level of accuracy is obtained.

Figure 4 illustrates the sound transmission loss results of a double MPP structure under sound excita-
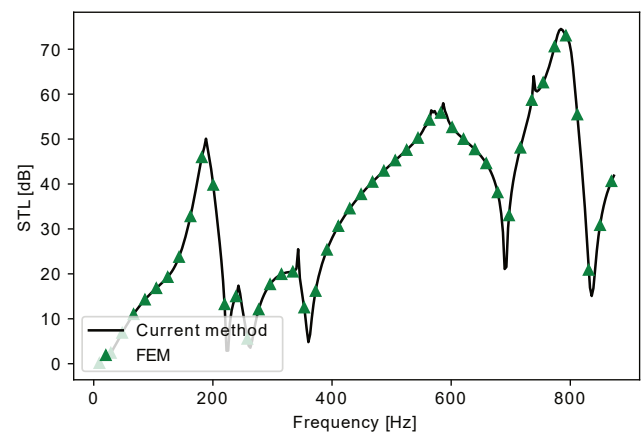
Fig. 4. Comparison of calculated STLs using the present approach and FEM results for double MPP coupled to a receiving enclosure.

tion using the current approach and FEM simulation. As depicted, the STL predictions obtained through the present technique align closely with the results obtained through FEM simulation, demonstrating good agreement between the two methods.

Figure 5 illustrates the STL results of a double MPP structure when connected to a receiving and source enclosure was examined using the current approach alongside FEM simulations. As illustrated, the STL derived from the current method employed in this study agrees with the outcomes obtained through the FEM simulation.
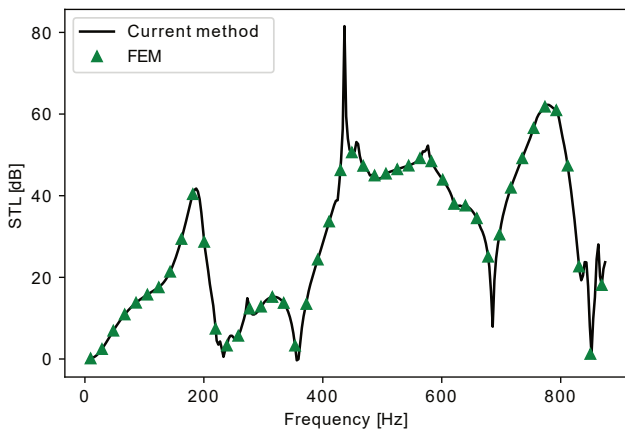
Fig. 5. Comparison of calculated STLs using the present approach and FEM results for double MPP coupled to both the receiving and source enclosure.

4.2. Comparison with impedance tube

Comparisons are made between the predicted TL when the finite partition is mounted on a rectangular impedance tube, and when it is coupled to acoustic enclosures. Particularly, we have selected the study provided by KIM *et al.* (2020b), which examines the propagation of two-dimensional plane waves over an insulating partition of a finite size 0.26×0.21 m consisting of two flexible MPPs mounted on the rectangular Kundt tube separated by an air gap of 0.03 m with clamped supported boundaries. Simulations were conducted using the same physical parameters as in the selected study (KIM *et al.*, 2020b): the MPPs are made of aluminium with the following physical properties; Young's modulus of 7.2×10^{10} Pa, the density of 2700 kg/m^3, Poisson's ratio of 0.34, structural damping ratio of 0.01, 1 mm thickness, 0.8 mm diameter holes, and a perforation ratio of 0.05%. The chosen dimensions for the MPPs are 0.26×0.21 m. The dimension of the receiving acoustic enclosure is $L_x \times L_y \times h_e = 0.26$ m $\times 0.21$ m $\times 0.4$ m.

Figure 6 displays the findings for the TL when the double MPPs are excited by a plane wave coupled to a receiving enclosure, and when an emitting room is connected to the coupled system. Comparing these
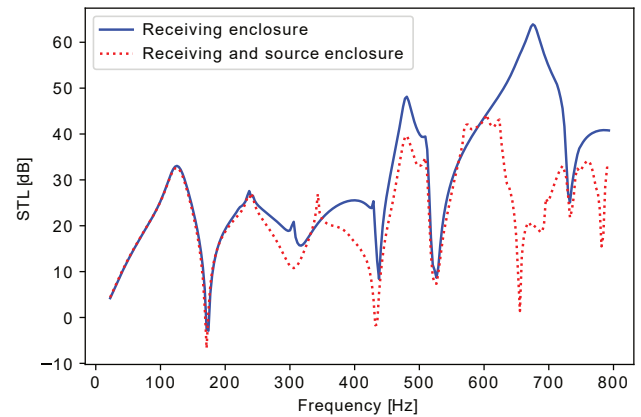
Fig. 6. Computed STL for double MPP coupled to acoustic enclosures using the same physical parameters as in (KIM *et al.*, 2020b).

findings to those of the finite double MPP partition put on an impedance tube reveals that the suggested modal formulation can predict the TL's general trend with high accuracy over a broad range of frequencies. Also, the STL is improved at plate-cavity-plate resonance in the coupled configuration similarly to the impedance tube case. It can be observed that there are visible and separated natural frequencies of the receiving room. As a result, intense dips and fluctuations marked the TL in addition to those presenting the modal behavior of the structure. However, it can be remarked that the STL is slightly degraded when coupled to an acoustic enclosure. The acoustic resonances present in the enclosure offer further information on the modal effects on the sound transmission. The TL drops turn negative (Fig. 6), while the TL remains positive in Kundt's tube example. This paradoxical feature is due to the resonance of the coupled system. To further study the effect of the source room on the transmission properties of the structure, a secondary enclosure is coupled to the multilayered MPPs as an emitting room. The dimensions of the source enclosure are $L_x \times L_y \times h_{e2} = 0.26$ m $\times 0.21$ m $\times 0.3$ m with a source strength $Q_0 = 10^{-4}$ m^3/s placed at $(0.15, 0.12, 0.2)$. From Fig. 6, the predicted TL for the multi-layered MPPs when it is connected to a source and receiving an enclosure. It can be seen that the modal behavior of the emitting room is still present at very low frequencies presented by the dips and fluctuations on the STL curve corresponding to the excited acoustic modes in both the source and receiving enclosures.

4.3. Parametric analysis

Numerical modeling is used to investigate the impact of various system parameters on the sound transmission of the double MPPs structure. Numerical analysis is employed to assess various critical system parameters. These include factors such as the dimensions

and impedance of the acoustic enclosure, the perforation ratio of the MPP, the thickness of the air gap, and the incorporation of absorbent materials within the gap. In the first case, the upper MPP is under acoustic excitation and an acoustic point source of strength $Q_0 = 10^{-4}$ m^3/s is placed at $(0.15, 0.12, 0.4)$ in the source room in the second. In numerical simulations, the dimensions of the coupled enclosures are defined as follows: the dimension of the enclosure is $L_x \times L_y \times h_{e1} = 0.5$ m $\times 0.35$ m $\times 0.6$ m, the dimension of the source enclosure when coupled to the system is $L_x \times L_y \times h_{e2} = 0.5$ m $\times 0.35$ m $\times 0.7$ m, and the physical properties of the MPPs are kept the same as in the previous section. The air gap depth (h_a) is 70 mm and the hole diameter is 0.3 mm.

4.3.1. Effect of acoustic enclosure dimensions on STL

To investigate the modal effects of both the receiving enclosure and emitting enclosure on STL, a set of numerical simulations with varying h_e is conducted. Figure 7 displays the impact of different receiving enclosure depths on the sound transmission loss of the double MPP structure when connected to an acoustic enclosure under acoustic excitation.
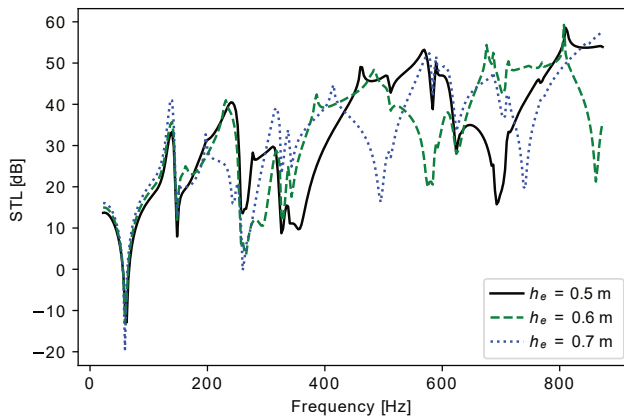
Fig. 7. Sound transmission loss of double MPP for different dimensions of receiving acoustic enclosure, $\sigma_1 = \sigma_2 = 0.1\%$.

Using the potential energy in the receiving chamber for calculation, Fig. 7 illustrates the corresponding transmission loss. The introduction of the receiving enclosure has notably influenced the previous results, primarily due to its modal properties playing a role. Below the first mode controlled by the enclosure, energy transmission is primarily influenced by structural resonances. The observable difference in the curves arises because the modes of the coupled enclosure amplify the mean square pressure within it for a given panel excitation. Additionally, changes in the enclosure size lead to modifications in the resonance frequencies, resulting in shifts in the dips corresponding to excited enclosure modes. It is worth noting that a decrease in the cavity depth results in an increase in the associated frequencies of the acoustical cavity, as seen in

Fig. 7. For instance, the dip generated by the acoustic mode at 678 shifts to 592 Hz when the depth changes from 0.5 to 0.6 m. In the second case when the double MPPs is connected to a source room, the depth of the emitting enclosure is varied (h_{e2} = 0.6, 0.7, and 0.8 m) while maintaining the receiving enclosure depth constant and equal to 0.6 m. It can be seen from Fig. 8 that additional dips and peaks are present. This can be explained by the sensitivity of the diffuseness of the acoustic field to many parameters such as the source position and the room geometry. The presence of receiving enclosure or a source and receiving enclosure wield a significant influence on the STL of double MPP structures. Hence, the transmission loss of double MPPs connected to acoustic enclosures necessitates thorough examination in each case.
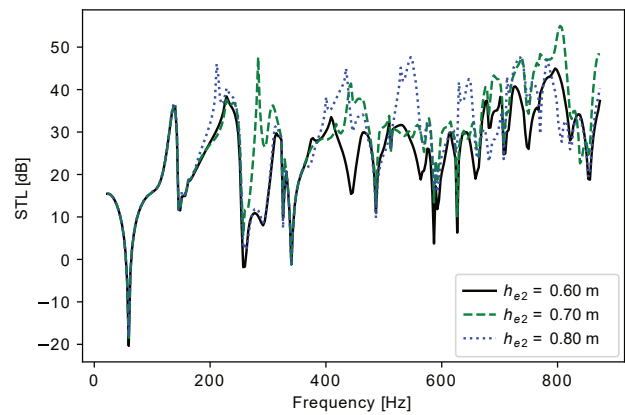
Fig. 8. Sound transmission loss of double MPP for different dimensions of source acoustic enclosure, $\sigma_1 = \sigma_2 = 0.1\%$.

4.3.2. Effect of acoustic enclosure impedance on STL

The coupled system transmits the acoustic excitation into the enclosure. The enclosure's boundary conditions may affect the acoustic properties of the enclosure and further influence the transmission of energy via the double MPP structure. Consequently, it is crucial to examine the influence of wall impedance on energy transmission. Figure 9 shows how the coupled
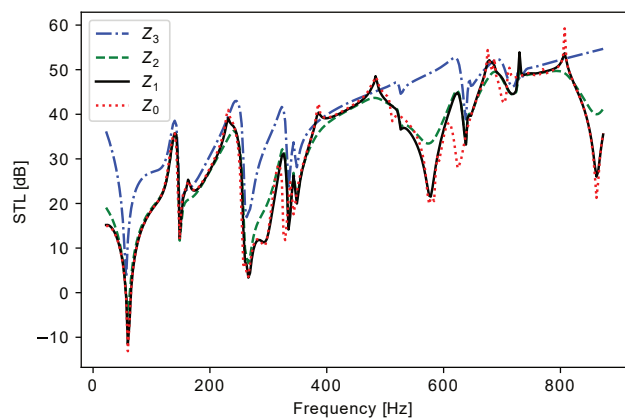
Fig. 9. Effect of impedance on STL, $\sigma_1 = \sigma_2 = 0.1\%$.

system's sound insulation properties change when the impedance is modified. Note that impedance boundary conditions are accounted for by modifying Eq. (2). The impact of the impedance's real component is investigated.

The influence of the real component of the impedance on the STL is shown in Fig. 9. STLs are computed with specified values of impedance $Z_0 = j \times 10^8$, $Z_1 = \rho_0 c (200 - 2j)$, $Z_2 = \rho_0 c (20 - j2)$, $Z_3 = \rho_0 c (2 - 2j)$. These three numbers represent the corresponding sound absorption coefficients: rigid, 0.04, 0.58, and 0.86. As can be observed in Fig. 9, the STL improves whenever there is a general rise in the sound absorption coefficient. In cases with very low absorption coefficients, the STL over the whole frequency spectrum that was investigated, is practically the same as that of rigid walls. More than 0.04 sound absorption, STL occurs mostly at the resonance frequencies of the enclosure but is largely unchanged at the initial resonant frequencies of the system. This is because the real component of the impedance increases sound transmission capabilities by enabling the cavity to dissipate energy more efficiently. At the resonant acoustic modes, it is thus plausible to conclude that the actual component of wall impedance has the greatest effect on sound transmission.

4.3.3. Effect of perforation ratio of the MPPs on STL

To investigate the effect of the perforation ratio on the multilayered MPPs for both cases (when the MPPs are coupled to the receiving room and when the MPP is coupled to both the receiving and emitting room), the STLs are plotted for different perforation ratio values. The micro-perforation ratios of the two MPPs are equal: $\sigma_1 = \sigma_2 = 0.0$, 0.05, 0.1, and 0.2%. As shown in Figs. 10 and 11, as the micro-perforation ratios grow, the STL deteriorates for both cases with a large gain at resonances.
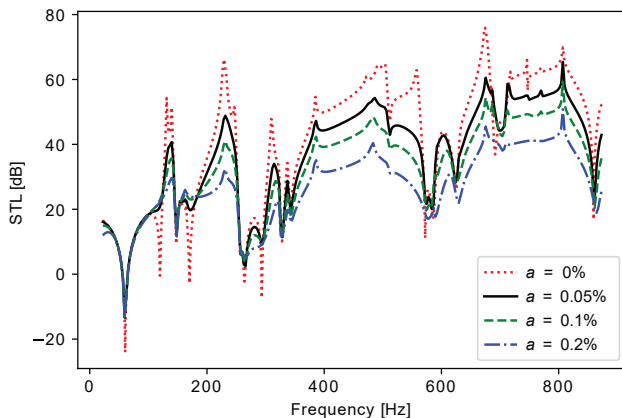
Fig. 10. STL of double MPPs connected to a receiving enclosure for various perforation ratios when $\sigma_1 = \sigma_2$.

Perforation ratios of the two MPPs are normally varied in a typical arrangement to reduce reflections
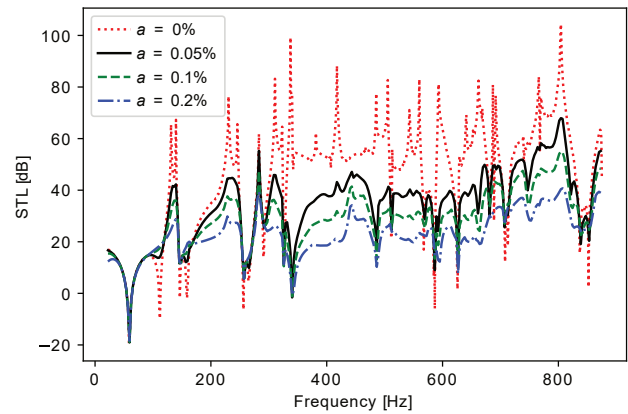
Fig. 11. STL of double MPPs connected to an emitting and receiving enclosure for various perforation ratios when $\sigma_1 = \sigma_2$.

and transmissions from internal noise sources such as those produced by the engine and sent into the passenger compartment or in adjacent rooms. Figure 12 illustrates the calculated STLs for various perforation ratios in the first case.
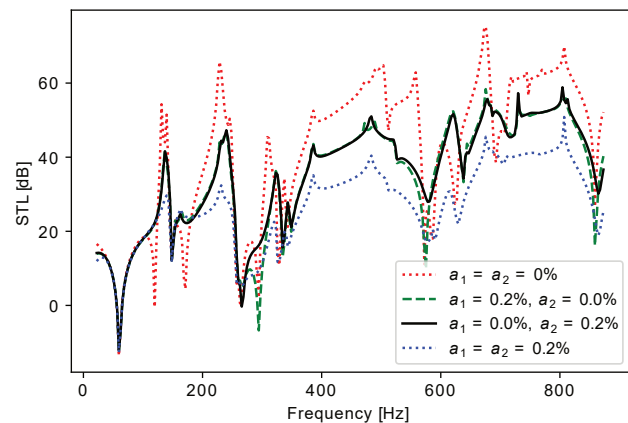
Fig. 12. STL of double MPPs connected to a receiving enclosure for various perforation ratios when $\sigma_1 \neq \sigma_2$.

Similar to the case of equal micro-perforation, the STLs deteriorate when the plate is perforated, as shown in Fig. 12. In addition, the STL is dependent on the variation of perforation ratios of the two MPPs, as illustrated in Fig. 12, for the case of (0.0, 0.2%) and (0.2, 0.0%). However, a large gain is obtained at resonances with the arrangement (0.0, 0.2%).

Figure 13 displays the sound transmission loss when the double MPPs is coupled to both the source and receiving enclosures. Acoustic resonances in the receiving chamber (dips) are attenuated when the perforations are located on the receiving side (0.0, 0.2%). Similarly, acoustic resonances in the source enclosure (peaks) are also damped when the perforations are positioned on the source side (0.2, 0.0%). For the arrangement (0.2, 0.2%), the resonances of both the receiving and source enclosure are damped. However, the sound transmission loss is highly degraded.
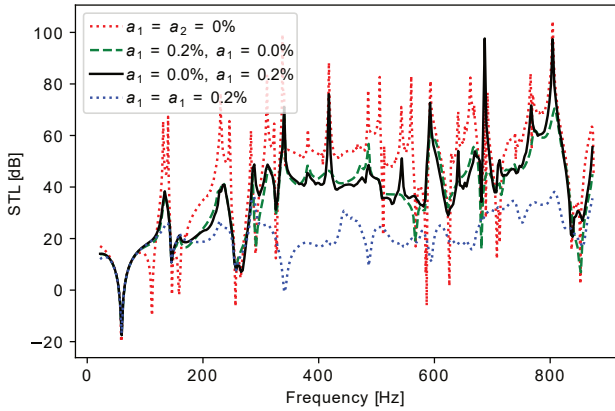
Fig. 13. STL of double MPPs connected to an emitting and receiving enclosure for various perforation ratios when $\sigma_1 \neq \sigma_2$.

4.3.4. Effect of the gap thickness

To assess the influence of varying air gap depths on STL, a series of numerical simulations were conducted. Figures 14 and 15 illustrate how the STL of a double MPP structure responds to different air gap depths
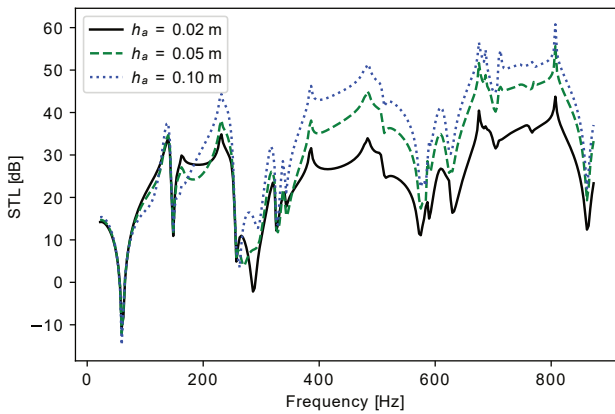
Fig. 14. Influence of air gap on STL of double MPP partition, $\sigma_1 = \sigma_2 = 0.1\%$.
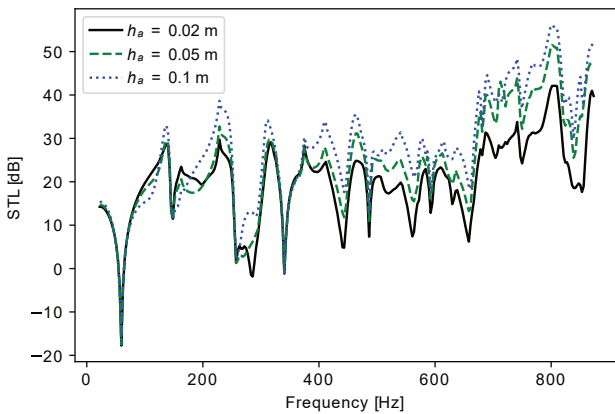
Fig. 15. Influence of air gap on STL of double MPP partition when coupled to both source and receiving enclosure, $\sigma_1 = \sigma_2 = 0.1\%$.

(0.02, 0.05, and 0.10 m) when subjected to acoustic excitation and when it is coupled to both the source and receiving room. As depicted in Figs. 14 and 15, as the air gap thickness increases, the STL values increase. This phenomenon is attributed to an increase of system coupling resulting from the reduced air gap thickness. As the air gap thickness rises, Figs. 14 and 15 demonstrate that the transmission characteristics in the case when coupled to a receiving chamber increase greater than those of the second case. Thus, each case should be carefully considered. In conclusion, the thickness of the air gap significantly affects the sound insulation capabilities of the structure. In the case, when the partition is coupled to both the receiving and source enclosure the dissipation properties are significant when the air gap is increased.

4.3.5. Influence of porous material on sound transmission loss

To enhance the sound transmission loss at resonant frequencies, we introduce sound-absorbing material with a specific flow resistivity into the space between the MPPs. This absorbent material is represented as an equivalent fluid, and its material characteristics are determined using the empirical model developed by DELANY and BAZLEY (1970). The associated weak form (Eq. (15)) may account for airborne propagation through low frame stiffness insulating materials filling the cavity, by replacing c_0 and ρ_0 with c_a and ρ_a which are complex and frequency-dependent. It is important to note that for a comprehensive description, poroelastic modeling should be considered. However, as demonstrated by BERANEK in 1947, when sound propagates through soundproofing materials with relatively low frame stiffness, longitudinal elastic vibrations attenuate significantly more than acoustic compression waves.

Figure 16 presents a comparison of computational results for a gap filled with fiberglass as opposed to air for the case when the partition is coupled to both the
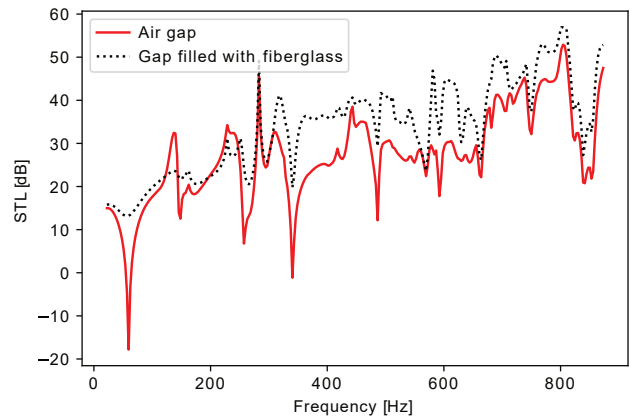
Fig. 16. Computed STLs for gap filled with fiberglass and gap filled with air.

receiving and source enclosure. The findings reveal an increase in transmission loss. Notably, significant gains are observed at resonance points. The system's response is predominantly influenced by the damping introduced by the absorbent material. This damping is primarily attributed to acoustic dissipation resulting from viscous drag forces and thermal interactions between the air and the material.

4.4. Sound transmission loss of triple MPPs

In Figs. 17 and 18, we have plotted the sound transmission loss for different perforation ratios for the two cases. The respective thicknesses and hole diameters of the three MPPs are consistent at $h_1 = h_2 = h_3 = 1$ mm and $d_1 = d_2 = d_3 = 0.3$ mm, with cavity depths equal to $h_{a1} = h_{a2} = 40$ mm. The dimensions of the enclosures remain unchanged.
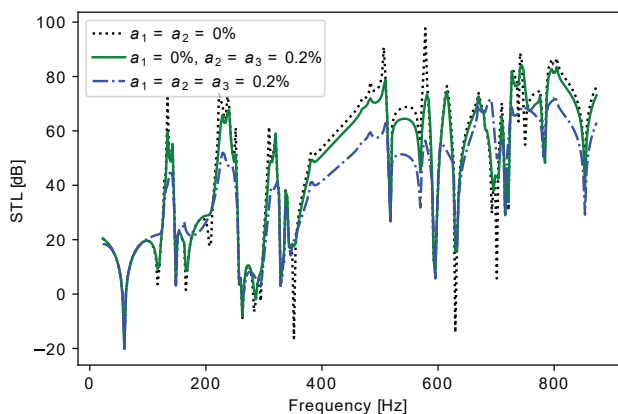
Fig. 17. STL of triple MPPs for various perforation ratios of the MPP when coupled to the receiving enclosure.
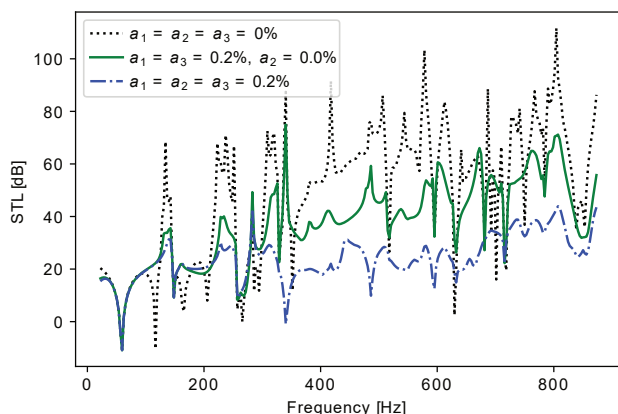
Fig. 18. STL of triple MPPs for various perforation ratios of the MPP when coupled to both receiving and source enclosure.

As observed with double MPPs, the modal effect of the acoustic enclosure is present and the STL values tend to decrease as the micro-perforation ratio increases, except at the resonant frequencies of the coupled system where large gain is obtained.

5. Conclusion

This study presents the results of a vibro-acoustic investigation of a double MPP structure coupled to receiving enclosure or both the source and receiving enclosure. The transmission loss of this structure was predicted using an analytical methodology. Using a modified variational model, the equations governing the coupled system were derived. The acoustic pressure within the enclosures is described by the 3D-enhanced Fourier series. Furthermore, the validity and precision of this model were confirmed through FE computations, resulting in a substantial level of agreement. Then a parametric analysis was carried out aimed at discerning the influence of enclosure size, air gap thickness, acoustic enclosure impedance, perforation ratio of the MPPs, and insertion of absorbent material in the gap on the sound transmission of double MPPs in the coupled configurations.

The results summarized here are the most significant. It has been shown that the presence of an acoustic enclosure on the receiving side or both sides may have a significant effect on the sound transmission loss of double MPP structures, resulting in additional dips and peaks associated with the excited acoustic modes of both the source and receiving enclosure. In addition, the real component of the wall impedance dissipates the energy of the enclosure to affect the sound transmission over the double MPP structure, and thus primarily influences the sound transmission at the natural frequencies of the enclosure. As expected, the STLs deteriorate with the increase of the micro-perforation ratio of the plate with a gain at resonances. In the case where the double MPP is coupled to both the receiving and emitting enclosure, the sound transmission loss is damped at acoustic resonances in the two enclosures. Furthermore, it was found that as the thickness of the air gap increases, the Sound Transmission Loss values also increase pointing out that there is difference in the increase in STL between the two situations. Additionally, the insertion of absorbent material into the gap, in the case where the partition is coupled to both an emitting enclosure and receiving enclosure, leads to an increase in transmission loss, especially at resonance points. In the case of triple MPPs, we observe consistent behavior. Furthermore, when excited by a plane wave and connected to an acoustic enclosure, the plate-MPP-MPP structure demonstrated optimal performance. On the other hand, the MPP-plate-MPP configuration exhibited good performance when connected to both receiving and source enclosures.

The introduction of an acoustic enclosure on the receiving side or both sides can have a substantial effect on the sound transmission loss of double MPP structures. Hence, the transmission loss of double MPPs connected to acoustic enclosures necessitates thor-

ough examination in each case. Compared to earlier methods, this approach offers greater ease in defining various structural and acoustic boundary conditions. Moreover, the suggested method allows the direct application to more complex geometric models that only require coordinate transformation to transform irregular shapes into rectangles.

References

1. ALISAH M.I., OOI L.E., RIPIN Z.M., YAHYA A.F., HO K. (2021), Acoustic attenuation performance analysis and optimisation of expansion chamber coupled micro-perforated cylindrical panel using response surface method, *Archives of Acoustics*, **46**(3): 507–517, doi: 10.24425/aoa.2021.138143.

2. ALLAM S., ÅBOM M. (2011), A new type of muffler based on microperforated tubes, *Journal of Vibration and Acoustics*, **133**(3): 031005, doi: 10.1115/1.4002956.

3. BERANEK L.L. (1947), Acoustical properties of homogeneous, isotropic rigid tiles and flexible blankets, *The Journal of the Acoustical Society of America*, **19**(4): 556–568, doi: 10.1121/1.1916521.

4. BRAVO T., ELLIOTT S.J. (2004), Variability of low frequency sound transmission measurements, *The Journal of the Acoustical Society of America*, **115**(6): 2986–2997, doi: 10.1121/1.1738452.

5. BRAVO T., MAURY C., PINHÈDE C. (2012), Sound absorption and transmission through flexible microperforated panels backed by an air layer and a thin plate, *The Journal of the Acoustical Society of America*, **131**(5): 3853–3863, doi: 10.1121/1.3701987.

6. BRAVO T., MAURY C., PINHÈDE C. (2014), Optimising the absorption and transmission properties of aircraft microperforated panels, *Applied Acoustics*, **79**: 47–57, doi: 10.1016/j.apacoust.2013.12.009.

7. BRAVO T., MAURY C., PINHÈDE C. (2016), Optimisation of micro-perforated cylindrical silencers in linear and nonlinear regimes, *Journal of Sound and Vibration*, **363**: 359–379, doi: 10.1016/j.jsv.2015.11.011.

8. CARNEAL J.P., FULLER C.R. (2004), An analytical and experimental investigation of active structural acoustic control of noise transmission through double panel system, *Journal of Sound and Vibration*, **272**(3–5): 749–771, doi: 10.1016/S0022-460X(03)00418-8.

9. CHAZOT J.-D., GUYADER J.-L. (2007), Prediction of transmission loss of double panels with a patch-mobility method, *The Journal of the Acoustical Society of America*, **121**(1): 267–78, doi: 10.1121/1.2395920.

10. CHENG L., LI Y.Y., GAO J.X. (2005), Energy transmission in a mechanically-linked double-wall structure coupled to an acoustic enclosure, *The Journal of the Acoustical Society of America*, **117**(5): 2742–2751, doi: 10.1121/1.1886525.

11. CHIEN W.Z. (1983), Method of high-order Lagrange multiplier and generalized variational principles of elasticity with more general forms of functional, *Applied Mathematics and Mechanics*, **4**: 143–157, doi: 10.1007/BF01895439.

12. DELANY M.E., BAZLEY E.N. (1970), Acoustical properties of fibrous materials, *Applied Acoustics*, **3**(2): 105–116, doi: 10.1016/0003-682X(70)90031-9.

13. DU J.T., LI W.L., LIU Z.G., XU H.A., JI Z.L. (2011), Acoustic analysis of a rectangular cavity with general impedance boundary condition, *The Journal of the Acoustical Society of America*, **130**(9): 807–817, doi: 10.1121/1.3605534.

14. DUPONT T., PAVIC G., LAULAGNET B. (2003), Acoustic properties of lightweight micro-perforated plate systems, *Acta Acustica united Acustica*, **89**(2): 201–212.

15. FALSAFI I., OHADI A. (2018), Optimisation of multistep cavity configuration to extend absorption bandwidth of micro perforated panel absorber, *Archives of Acoustics*, **43**(2): 187–195, doi: 10.24425/122366.

16. FUCHS H.V., ZHA X. (1997), Acrylic-glass sound absorbers in the plenum of the deutscher bundestag, *Applied Acoustics*, **51**(2): 211–217, doi: 10.1016/S0003-682X(96)00064-3.

17. GAGLIARDINI L., ROLAND J., GUYADER J.L. (1991), The use of a functional basis to calculate acoustic transmission between rooms, *Journal of Sound and Vibration*, **145**(3): 457–478, doi: 10.1016/0022-460X(91)90114-Y.

18. KANG J., BROCKLESBY M.W. (2005), Feasibility of applying micro-perforated absorbers in acoustic window systems, *Applied Acoustics*, **66**(6): 669–689, doi: 10.1016/j.apacoust.2004.06.011.

19. KIHLMAN T. (1967), Sound radiation into a rectangular room. Applications to airborne sound transmission in buildings, *Acta Acustica*, **18**(1): 11–20.

20. KIM H.-S., KIM S.-R., KIM B.-K., MA P.-S., SEO Y.-H. (2020a), Sound transmission loss of multilayered infinite micro-perforated plates, *The Journal of the Acoustical Society of America*, **147**(1): 508–515, doi: 10.1121/10.0000600.

21. KIM H.-S., MA P.-S., KIM B.-K., LEE S.-H., SEO Y.-H. (2020b), Sound transmission loss of multi-layered elastic micro-perforated plates in an impedance tube, *Applied Acoustics*, **166**: 107348, doi: 10.1016/j.apacoust.2020.107348.

22. KROPP W., PIETRZYK A., KIHLMAN T. (1994), On the meaning of the sound reduction index at low frequencies, *Acta Acustica* (*Les Ulis*), **2**(5): 379–392.

23. LIU Z., ZHAN J., FARD M., DAVY J.L. (2017), Acoustic properties of multilayer sound absorbers with a 3D printed micro-perforated panel, *Applied Acoustics*, **121**: 25–32, doi: 10.1016/j.apacoust.2017.01.032.

24. LØVHOLT F., NORÈN-COSGRIFF K., MADSHUS C., ELLINGSEN S.E. (2017), Simulating low frequency sound transmission through walls and windows by a two-way coupled fluid structure interaction model, *Journal of Sound and Vibration*, **396**: 203–216, doi: 10.1016/j.jsv.2017.02.026.

25. MAA D.-Y. (1998), Potential of microperforated panel absorber, *The Journal of the Acoustical Society of America*, **104**(5): 2861–2866, doi: 10.1121/1.423870.

26. MENG H., GALLAND M.A., ICHCHOU M., BAREILLE O., XIN F.X., LU T.J. (2017), Small perforations in corrugated sandwich panel significantly enhance low-frequency sound absorption and transmission loss, *Composite Structures*, **182**: 1–11, doi: 10.1016/j.compstruct.2017.08.103.

27. MENG H., GALLAND M.A., ICHCHOU M., XIN F.X., LU T.J. (2019), On the low-frequency acoustic properties of novel multifunctional honeycomb sandwich panels with micro-perforated faceplates, *Applied Acoustics*, **152**: 31–40, doi: 10.1016/j.apacoust.2019.02.028.

28. MU R.L., TOYODA M., TAKAHASHI D. (2011a), Improvement of sound insulation performance of multilayer windows by using microperforated panel, *Acoustical Science and Technology*, **32**(2): 79–81, doi: 10.1250/ast.32.79.

29. MU R. L., TOYODA M., TAKAHASHI D. (2011b), Sound insulation characteristics of multi-layer structures with a microperforated panel, *Applied Acoustics*, **72**(11): 849–855, doi: 10.1016/j.apacoust.2011.05.009.

30. MULHOLLAND K.A., LYON R.H. (1973), Sound insulation at low frequencies, *The Journal of the Acoustical Society of America*, **54**(4): 867–878, doi: 10.1121/1.1914340.

31. OSIPOV A., MEES P., VERMEIR G. (1997a), Numerical simulations of airborne sound transmission at low frequencies: The influence of the room and the partition parameters, [in:] *Proceedings of InterNoise 97*, pp. 759–762.

32. OSIPOV A., MEES P., VERMEIR G. (1997b), Low-frequency airborne sound transmission through single partitions in buildings, *Applied Acoustics*, **52**(3–4): 273–288, doi: 10.1016/S0003-682X(97)00031-5.

33. PFRETZSCHNER J., COBO P., SIMÓN F., CUESTA M., FERNÁNDEZ A. (2006), Microperforated insertion units: An alternative strategy to design microperforated panels, *Applied Acoustics*, **67**(1): 62–73, doi: 10.1016/j.apacoust.2005.05.005.

34. QU Y.G., HUA H.X., MENG G. (2013a), A domain decomposition approach for vibration analysis of isotropic and composite cylindrical shells with arbitrary boundaries, *Composite Structures*, **95**: 307–321, doi: 10.1016/j.compstruct.2012.06.022.

35. QU Y.G., CHEN Y., LONG X.H., HUA H.X., MENG G. (2013b), A modified variational approach for vibration analysis of ring-stiffened conical–cylindrical shell combinations, *European Journal of Mechanics – A/Solids*, **37**: 200–215, doi: 10.1016/j.euromechsol.2012.06.006.

36. TAKAHASHI D., TANAKA M. (2002), Flexural vibration of perforated plates and porous elastic materials under acoustic loading, *Journal of the Acoustical Society of America*, **112**(4): 1456-1464, doi: 10.1121/1.1497624.

37. TANG Y., XIN F., HUANG L., LU T.J. (2017), Deep subwavelength acoustic metamaterial for low-frequency sound absorption, *Europhysics Letters*, **118**(4): 44002, doi: 10.1209/0295-5075/118/44002.

38. TANG Y., XIN F., HUANG L., LU T.J. (2019), Sound absorption of micro-perforated sandwich panel with honeycomb-corrugation hybrid core at high temperatures, *Composite Structures*, **226**: 111285, doi: 10.1016/j.compstruct.2019.111285.

39. TOYODA M., TAKAHASHI D. (2008), Sound transmission through a microperforated-panel structure with subdivided air cavities, *The Journal of the Acoustical Society of America*, **124**(6): 3594–3603, doi: 10.1121/1.3001711.

40. XIN F.X., LU T.J., CHEN C.Q. (2008), Vibroacoustic behavior of clamp mounted double-panel partition with enclosure air cavity, *The Journal of the Acoustical Society of America*, **124**(6): 3604–3612, doi: 10.1121/1.3006956.

41. YANG C., CHENG L. (2016), Sound absorption of microperforated panels inside compact acoustic enclosures, *Journal of Sound and Vibration*, **360**: 140–155, doi: 10.1016/j.jsv.2015.09.024.

42. YU X., CHENG L., YOU X. (2015), Hybrid silencers with micro-perforated panels and internal partitions, *The Journal of the Acoustical Society of America*, **137**(2): 951–962, doi: 10.1121/1.4906148.